Preprint Title	Controlled Supramolecular Assemblies of Luminescent Tridentate Cyclometalated Alkynyl Gold (III) Amphiphiles in Aqueous Media
Authors	Kelvin Sze-Yim Cai, Brian Boyan Liu and Franco King-Chi Leung
Publication Date	14 Apr. 2026
Article Type	Full Research Paper
Supporting Information File 1	SI-BLOC-GA.pdf; 4.1 MB
ORCID® iDs	Franco King-Chi Leung - https://orcid.org/0000-0003-0895-9307

Controlled Supramolecular Assemblies of Luminescent Tridentate Cyclometalated Alkynyl Gold (III) Amphiphiles in Aqueous Media

Kelvin Sze-Yim Cai[1], Brian Boyan Liu[1], and Franco King-Chi Leung*[1,2]

Address: [1]Department of Applied Biology and Chemical Technology, Research Institute of Future Food, The Hong Kong Polytechnic University, Hong Kong, China and [2]Centre for Eye and Vision Research, 17W Hong Kong Science Park, Hong Kong, China

Email: Franco King-Chi Leung – kingchifranco.leung@polyu.edu.hk

* Corresponding author

Abstract

Gold (III) complexes and amphiphiles have been extensively investigated over a decade. Supramolecular assemblies of the gold (III) amphiphiles in aqueous media exhibit high sensitivities to external stimulations for soft functional materials. Herein, we introduce a new molecular design of tridentate cyclometalated gold (III) amphiphile (**GA**) with flexible molecular structure modifications. Counterion exchange with sodium tosylate induces notable luminescent enhancement and enables controls over supramolecular assembly process. This approach drives a supramolecular assembly transformation of **GA** from disordered nanosheets to well-ordered nanoribbons upon

additions of multiple equivalents of counterion, enabling a tunable pathway for controlled supramolecular transformation.

Keywords

Amphiphiles; Gold (III) complex; Luminescence; Self-assembly; Supramolecular chemistry

Introduction

Supramolecular assemblies in natural systems, such as lipid bilayers and protein complexes, play essential roles in maintaining proper biological functions [1-3]. These natural structures have inspired developments of artificial supramolecular systems that offer structural diversity through delicate designed non-covalent interactions [4-7]. Amphiphilic molecules combine hydrophilic and hydrophobic groups. The intrinsic dual nature enables the molecules spontaneously assembling into well-defined nanostructures, such as micelles, vesicles, and nanotubes [7-9]. Through implementations of various stimuli-responsive molecular motifs, amphiphiles can respond to external stimuli, such as light, pH, and heat [4, 10-34], in allowing important biomedical applications, such as, drug delivery and cancer immunotherapy [35, 36]. An alternative molecular design approach is to incorporate organometallic complexes into amphiphile designs, thereby combining the advantageous functional properties of inorganic centers with the self-assembled structural properties of amphiphiles [37-41].

Gold (III) complexes have found in wide applications for catalysis [42-44], optoelectronic materials [45, 46], and bioconjugation methodologies [47-49], in considering the unique luminescence properties and excellent aqueous stability.

Amphiphilic gold (III) complexes were firstly reported by Che in 2016, which introduced polyethylene glycol (PEG)-functionalized gold (III) complexes to improve the biocompatibility and aqueous solubility [50]. Later, Che and co-workers developed charged cyclometalated gold (III) complexes, achieving kinetically controlled self-assembly in mixed solvents of acetonitrile and water through controls of counterions and its concentration [51]. Yam and co-workers have reported multi-responsive luminescent cationic gold (III) amphiphiles with the self-assembly process in mixed organic solvents [52]. These reports demonstrate remarkable structural sensitivities to gold (III) amphiphiles molecular designs and the resulting nanostructural changes. In general, gold (III) complexes have been suffered with low luminescent properties due to the intrinsic low-energy *d–d* ligand field states and the enriched electrophilicity of the gold (III) metal center. The non-emissive low-lying *d–d* state of gold (III) complexes quenches the luminescent excited state through thermal equilibrium and energy transfer [53]. Cyclometalated gold (III) complexes incorporated with strong σ-donating alkynyl ligands, reported by Yam, exhibit enhanced luminescent properties under ambient conditions, which is attributed to the strong *σ*-donating alkynyl ligands [54-58].

Our research team has developed bidentate cyclometalated gold (III) amphiphiles featured with counterion-controlled reversible assembly in aqueous media [59-61]. However, the synthetic complexity and aqueous solubility of these molecular designs have hindered the functional applicability towards biomaterials. We herein propose a new class of cyclometalated gold (III) amphiphiles (**GA**) with advanced accessibility and flexibility of the molecular structural modifications. Tridentate (C^N^C) cyclometalated gold (III) complex core is connected to a strong *σ*-donating alkyny-ligand, enabling luminescence of **GA** in aqueous media and ambident conditions. A propargyl group is linked to a terminal quaternary ammonium group through a nonyl-

linker, thereby enhancing the aqueous solubility of **GA**. Supramolecular nanostructures can be controlled by counterion exchange, through fine adjustments of the packing parameter of **GA**. With meticulous investigations of self-assembly processes, photophysical properties, and counterion-dependent structural transformations of **GA**, a new molecular framework for counterion-controlled luminescent soft materials can be established towards biomedical and biomaterial applications.

Results and Discussion

Design and Synthesis of GA

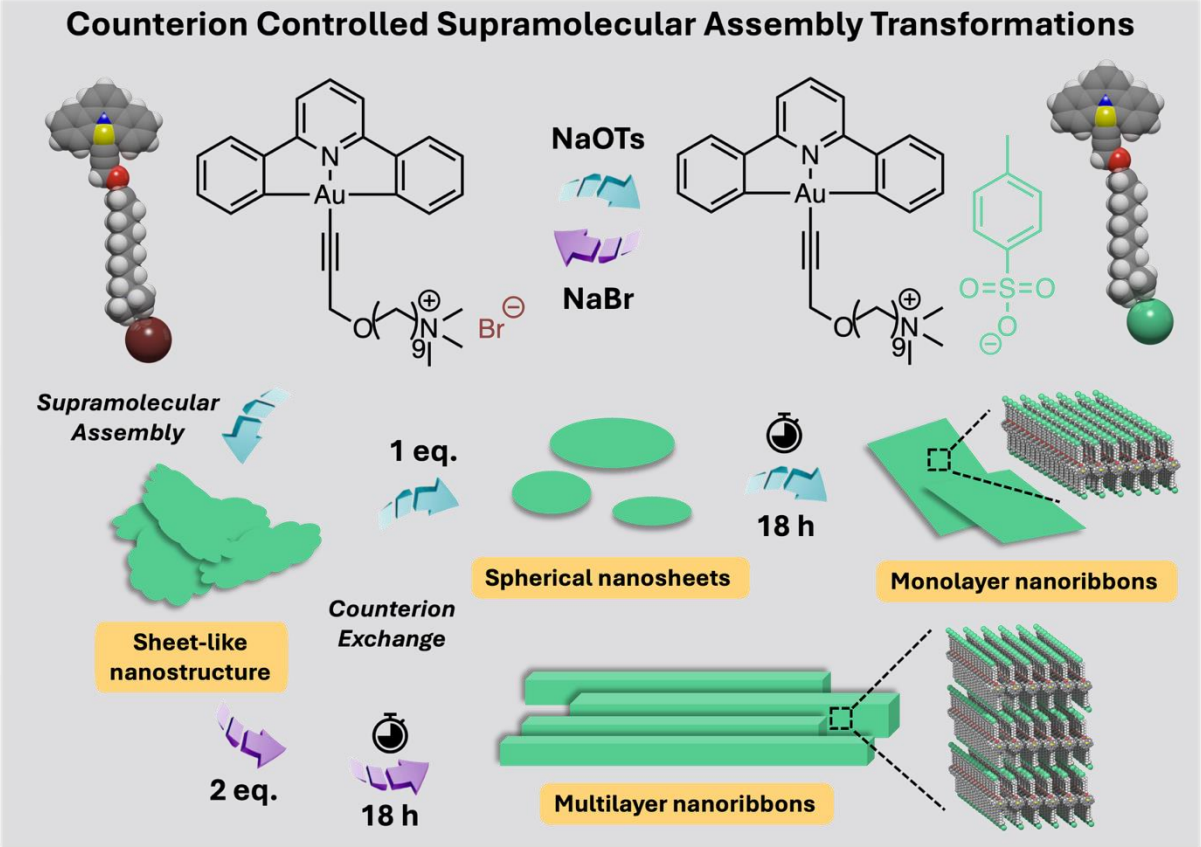

Scheme 1: Schematic illustration of design of **GA** and the corresponding supramolecular assembly transformations.

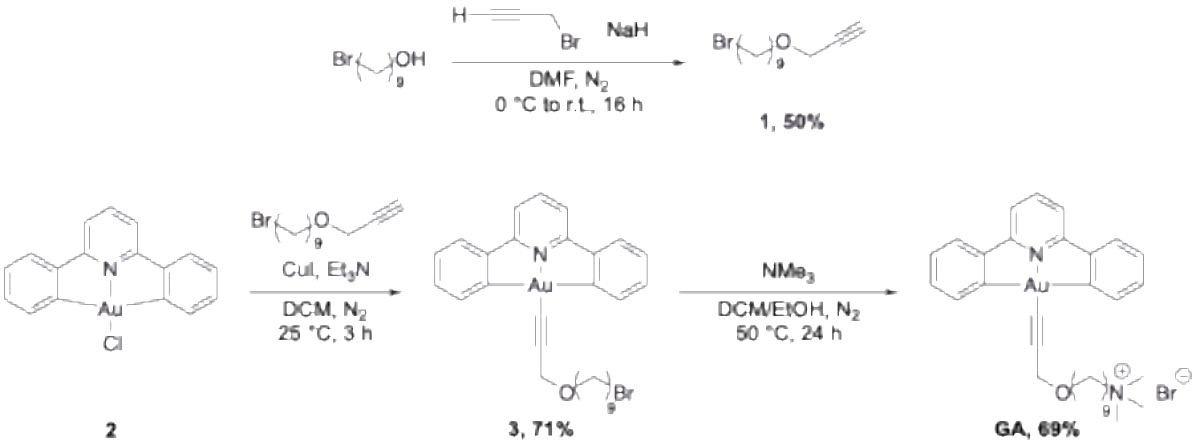

Scheme 2: Synthetic route of **GA**.

The gold amphiphile was designed with a tridentate (C^N^C) cyclometalated gold (III) complex core, which is functionalized with a *σ*-donating alkyny-ligand. A propargyl group was connected by a nonyl-linker with a quaternary ammonium ion as the charged end-group (Scheme 1). The synthetic route of **GA** is shown in Scheme 2. Compound **1** was obtained by the substitution of propargyl bromide with 9-bromo-1-nonanol. Based on the previously reported procedure, cyclometalated gold (III) complex **2** was synthesized and further reacted with compound **1** in the presence of triethylamine and catalytic amount of copper iodide to afford amphiphile-precursor **3**. The nucleophilic substitution of compound **3** with trimethylamine enabled to afford **GA**. The chemical structures of all newly synthesized compounds and **GA** were unambiguously characterized by ^{1}H-, ^{13}C-NMR, and high-resolution mass spectrometry (HRMS) (Figures S8–S13).

Photophysical Properties and Assembly of GA

A freshly prepared aqueous solution of **GA** (13.4 mM, 1.0 weight% (wt.%)) was annealed at 50.0 °C for 5 min and cooled to room temperature as the stock solution.

The stock solution of **GA** was diluted into a range of concentrations from 0.01 to 1.0 mM, in estimating the critical aggregation concentration (CAC) by static light scattering measurements (SLS). The CAC of **GA** was confirmed as 10 μM (Figure S1), representing plausible formations of **GA** supramolecular assemblies under aqueous environment. A diluted solution of **GA** (200 μM) was further thermally annealed by heating to 50.0 °C for 5 min and slowly cooling down to 20.0 °C at a rate of 1.0 °C/min. The UV-Vis absorption spectrum of the solution shows an intense absorption band at 304–318 nm and a moderately intense vibronic-structured absorption band at 360–405 nm at 20.0 °C (Figure 1a, black-line). The vibrational progressional spacings of 1300–1310 cm^{-1} in the lower energy band represent the skeletal vibrational frequencies of the cyclometalated C^N^C ligand. In considering the similar absorption bands observed in the cyclometalated gold (III) complex **2** [62] and the related alkynylgold (III) complexes [54-56], the vibronic-structured absorption band at 360–405 nm is revealed as insensitive to the structurally modified alkynyl-ligands, which is generally assigned as a metal-perturbed intraligand (IL) π-π^* transition of the C^N^C ligand. Subtle increase in absorbance with a hypochromic-shift of 3 nm was observed upon heating the solution to 50.0 °C (Figure 1a, red-line), which was reversed upon cooling to 20.0 °C. A methanol solution of **GA** (200 μM) shows no signs of spectral shift and is reversible upon annealing (Figure S2a), indicating the absence of supramolecular aggregation under organic environment and the thermal stability of **GA** in both organic and aqueous media.

Upon excitation with wavelength of 365 nm, a methanol solution of **GA** (200 μM) exhibits a broad and structureless emission band at 428 nm at 20.0 °C (Figure S2b, green-line). In contrast, an aqueous solution of **GA** (200 μM) exhibits an additional vibronic-structured emission band at 465–540 nm, and its emission intensity at 429 nm

(Figure 1b, green-line) is lower than that of **GA** in organic media (Figure S2b, green-line) at 20.0 °C. Given that a dichloromethane solution of cyclometalated gold (III) complex **2** (200 μM) shows significantly lowered emission intensity at 430 nm (Figure S3), the emission spectral results suggested that luminescent properties of **GA** have been greatly improved through a coupling with a σ-donor to gold (III) complex. Upon progressively heating the aqueous solution of **GA** from 10.0 °C to 50.0 °C, the resulting emission intensity of the vibronic-structured emission band was gradually decreased along with the subtly decreased structureless emission band at 428 nm (Figure 1b), possibly due to emissions from the **GA** assemblies.

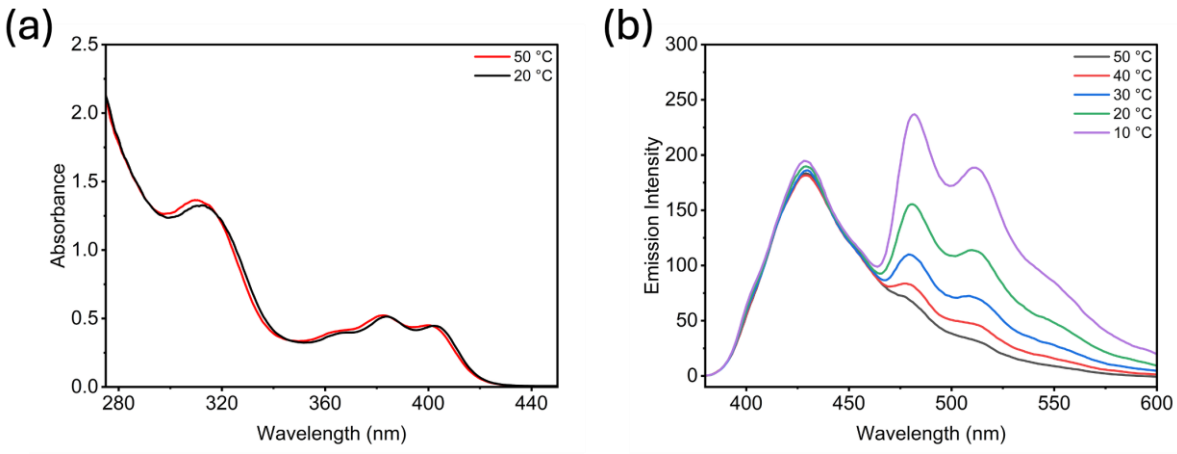

Figure 1: (a) UV-vis absorption spectra of **GA** (200 μM) in MQ water was cooled from 50.0 °C (red-line) to 20.0 °C (black-line) at a rate of 1.0 °C/min. (b) Emission spectra of **GA** (200 μM) in MQ water upon decreasing temperature from 50.0 °C (black-line) to 10.0 °C (purple-line).

Upon increasing the water content in methanol, the UV-vis absorption spectra of **GA** show a progressive increase in absorbance of the IL band tail at 420 nm (Figure S4a and S4b), suggesting formations of aggregates. The emission spectra of **GA** show a reduction in intensity of the structureless emission band at 429 nm with increased

emission of the lower-energy vibronic-structured emission band at 465–540 nm upon water content increased from 0% to 99% (Figure S4c and S4d). The obtained results demonstrated a clear redistribution of emission intensity due to aggregations of **GA** under aqueous media. Rigid molecular packed structures of **GA** in the aggregated form restrict intramolecular vibrations of the C^N^C ligand and suppress non-radiative decay pathways to activate the lower-energy emission. Essentially identical emission spectrum was observed in the methanol solution of **GA** at 20.0 °C (Figure S2b, green-line) to that of aqueous solution of **GA** (Figure 1b, black-line). This can be illustrated by the vibronic-structured emission band quenched at increased temperature and organic media due to possible non-radiative decay pathways. These results further confirmed that the vibronic-structure emission band can be induced upon **GA** assembly, which shows possible correlations with temperature and water content.

Counterion Controlled Supramolecular Assembly Transformations of GA

Negative-stained transmission electron microscopy (TEM) was used to analyze the assembled nanostructure of **GA**. TEM images of a thermal annealed aqueous solution of **GA** (2.68 mM, 0.2 wt.%) were revealed sheet-like nanostructures with widths ranging from hundreds of nanometers to micrometers (Figure 2a). A thermal annealed aqueous solution of **GA** (200 μM) was added with varying equivalents of aqueous solution of sodium tosylate (1.0, 2.0, and 4.0 equiv.), and subsequently heated to 50.0 °C and slowly cooled to 20.0 °C at a rate of 1.0 °C/min. UV-vis absorption spectra of the solution show a progressive bathochromic shift with increasing sodium tosylate equivalent (Figure 2b). The presence of isosbestic points at 359 nm, 375 nm, 381 nm, 395 nm, and 401 nm within the vibronic-structured absorption band indicates a selective counterion exchange process, where the organic tosylate anion replaces the inorganic bromide anion. The corresponding emission spectra of the solution show a

notable enhancement in overall intensity upon the addition of 1.0–2.0 equiv. of sodium tosylate (Figure 2c red-line and blue-line). However, the vibronic-structured emission band diminishes upon the addition of 4.0 equiv. of sodium tosylate (Figure 2c, green-line).

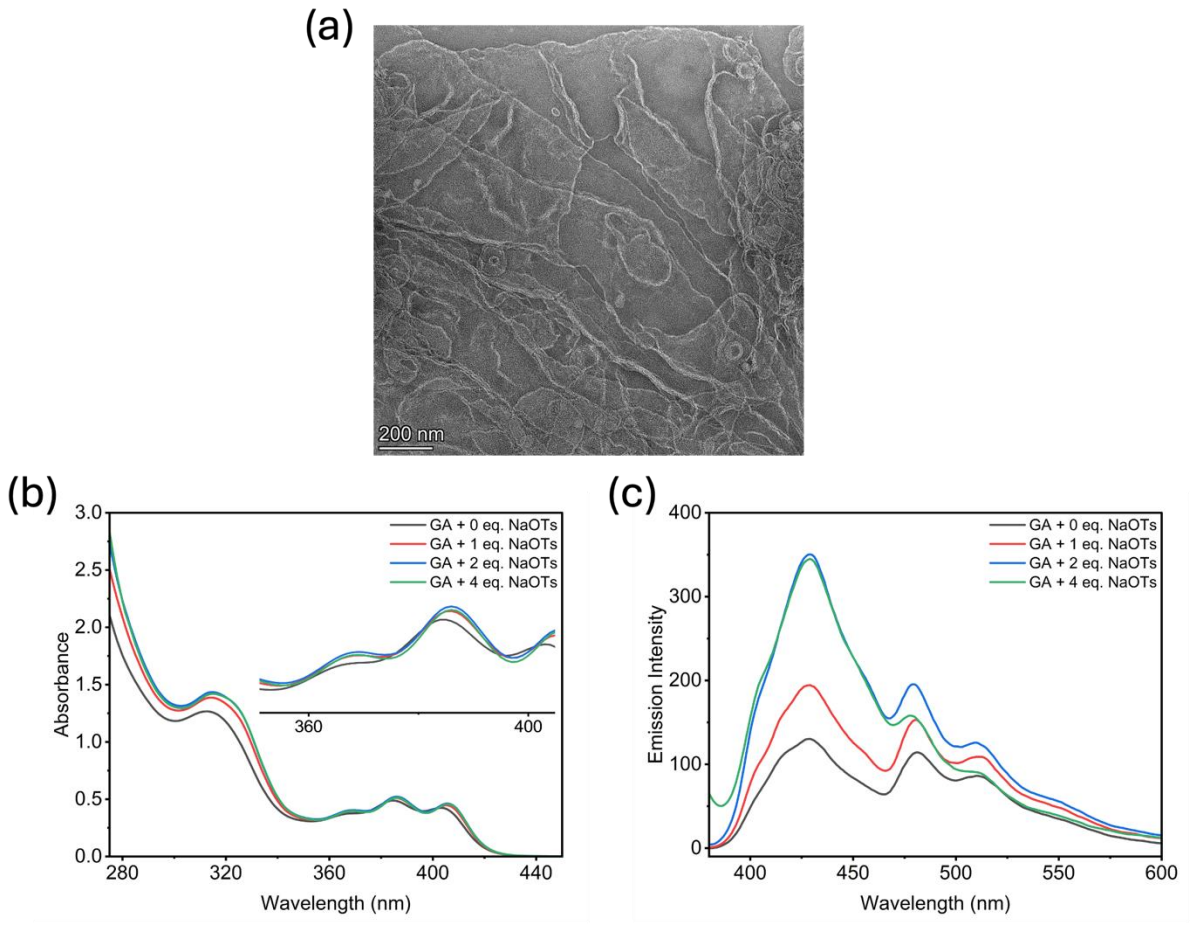

Figure 2: (a) TEM image of thermal annealed aqueous solution of **GA** (2.68 mM). (b) UV-vis absorption spectra and (c) emission spectra of **GA** (200 μM) in MQ water at 20.0 °C after addition of sodium tosylate (1.0, 2.0, and 4.0 equiv.).

The time-dependent UV-vis adsorption spectra of the annealed solution of **GA** without the addition of with sodium tosylate show no significant changes after 18 h at 20.0 °C (Figure S5a). In contrast, the absorbance of the annealed solution of **GA** with 1.0, 2.0

and 4.0 equiv. of sodium tosylate gradually increased after 18 hours of aging (Figure 3a, S5b, and S5c), indicating the formation of thermodynamic-driven assembly. A clear lag time for **GA** with tosylate (1.0 equiv.) suggests the presence of a metastable assembly state (Figure 3b, red-line). The spontaneous assembly process is suppressed due to the intermolecular interactions between the **GA** cation end group and the tosylate anion is stronger than the bromide anion [51, 63]. Increasing the concentration of sodium tosylate from 1.0 to 4.0 equiv. progressively reduces the lag time and accelerates the assembly process (Figure 3b). Notably, the final absorbance intensity of **GA** with tosylate (2.0 and 4.0 equiv.) is approximately twice that of **GA** with tosylate (1.0 equiv.), suggesting a significant difference in the density or size of thermodynamic-driven assemblies formed (Figure 3b).

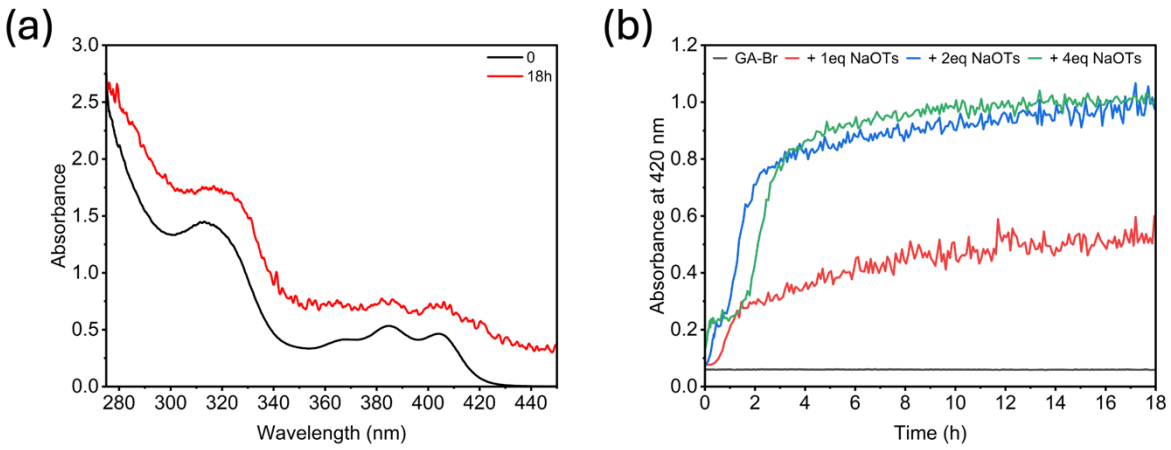

Figure 3: (a) Time-dependent UV-vis adsorption spectra of **GA** (200 μM) with addition of 1.0 equiv. of sodium tosylate in MQ water at 20.0 °C. (b) Time-dependent absorbance changes of **GA** at 420 nm with and without the addition of sodium tosylate.

A thermal annealed aqueous solution of **GA** (2.68 mM, 0.2 wt.%) with tosylate (1.0 equiv.) was imaged with spherical nanosheets with diameter (~200 nm–2 μm) as freshly prepared (Figure 4a). After aged for 18 h, the spherical nanosheets of **GA** have

evolved into stacked nanoribbons (Figure 4b). The time-dependent transitions indicate a kinetically controlled assembly process, in which the initial metastable assemblies transform into their thermodynamic-driven assemblies. Upon addition of 2.0 equiv. of tosylate and aging for 18 h, long nanoribbons were observed (Figure 4c). In contrast, irregular assemblies were observed in aged **GA** solution with 4.0 equiv. of tosylate (Figure S6), possibly due to the disruption of ordered assemblies by supersaturated ions. Atomic force microscopy (AFM) was performed to further confirm the assembled nanostructure of the aged **GA** solution (2.68 mM, 0.2 wt.%) with tosylate (1.0 and 2.0 equiv.). Essentially identical nanoribbon structures were found with a uniform height of 3.8 nm and 25 nm (Figure 4d and 4e). Given that the molecular length of **GA** is estimated to be approximately 2.4 nm, it is assumed that the nanoribbons of **GA** with 1.0 equiv. of tosylate are monolayer in which two **GA** molecules exhibit head-to-tail stacking, while **GA** with 2.0 equiv. of tosylate forms multilayer nanoribbons. These results demonstrate that counterion exchange from bromide to tosylate enhances the packing parameter of **GA**, resulting in a transition from less ordered nanosheets to well-ordered nanoribbons. In considering the significant influence of counterions, **GA** (2.68 mM, 0.2 wt.%) with tosylate (1.0 and 2.0 equiv.) were added sodium bromide with corresponding equivalents and further thermally annealed. The TEM images of the solution revealed the reverse supramolecular transformation from regular nanoribbons to sheet-like nanostructures (Figure S7).

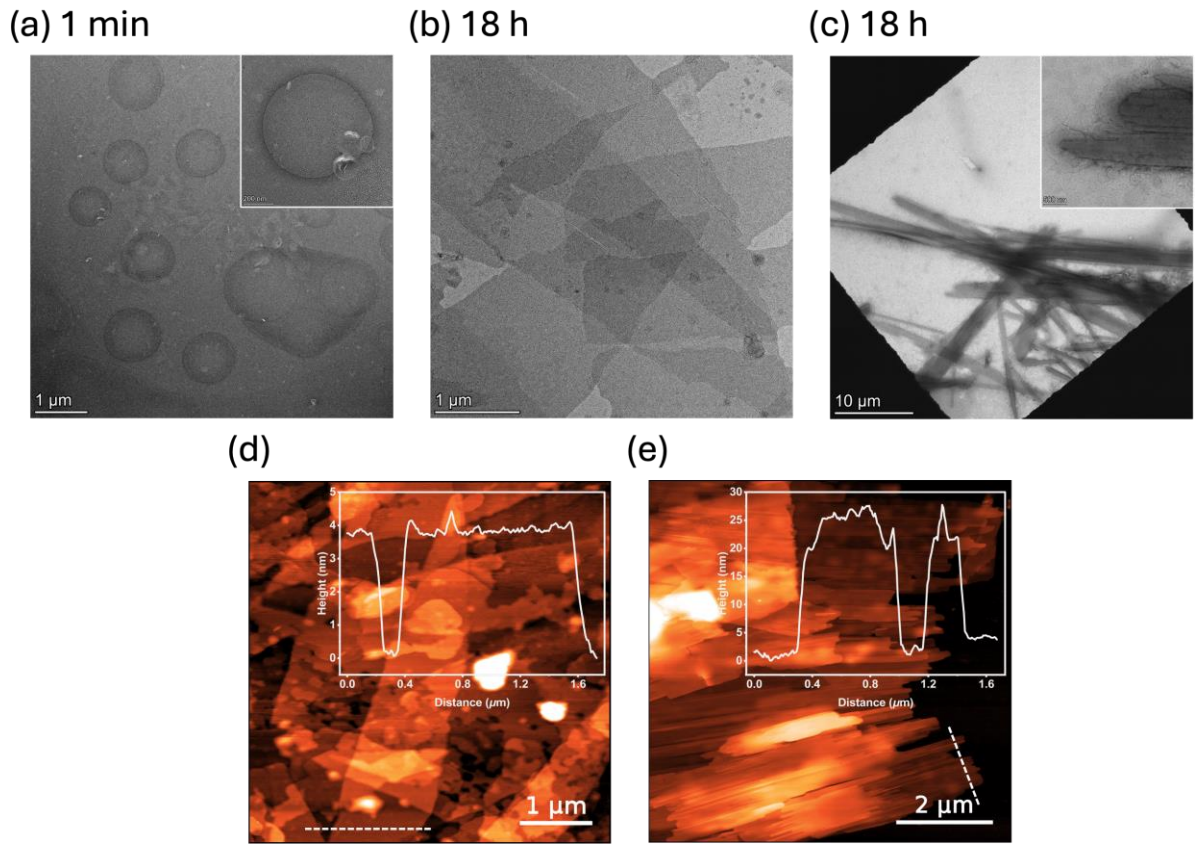

Figure 4: Time-dependent TEM changes of thermal annealed **GA** solution (2.68 mM) with the addition of 1.0 equiv. of sodium tosylate at (a) 1 min (inset: higher magnification of spherical nanosheets) and (b) 18 h. (c) TEM image of thermal annealed **GA** solution (2.68 mM) with the addition of 2.0 equiv. of sodium tosylate obtained at 18 h (inset: higher magnification of long nanoribbons). AFM images of the aged **GA** solution (2.68 mM) with the addition of (d) 1.0 equiv. and (e) 2.0 equiv. of sodium tosylate (inset: height profile along the indicated line).

Conclusion

Tridentate cyclometalated gold (III) amphiphile, functionalized with a σ-donating alkyny-ligand, was designed and synthesized. This structural modification significantly enhanced its luminescent properties in aqueous media. Supramolecular assembled

nanostructures of **GA** were imaged and confirmed by TEM and AFM. Upon addition of sodium tosylate, it enabled a thermodynamic-driven assembly process, leading supramolecular assembly transformations from sheet-like nanostructures to spherical nanosheets, and to stacked nanoribbons throughout an aging process. Well-defined monolayered and multilayered nanoribbons were observed by varying concentrations of tosylate ions. Reverse supramolecular transformation was enabled in the current gold (III) amphiphilic design by addition of bromide ions. The current system of tridentate cyclometalated gold (III) amphiphile lays the foundation for developing next generations of controlled supramolecular assembly of gold (III) amphiphiles.

Experimental

Materials: All commercial reagents were purchased from Acros Organics, Aladdin, Bidepharm, Dieckmann, Macklin and Tokyo Chemical Industry Co. Ltd, and were used as received unless otherwise specified. All reactions were performed under nitrogen unless otherwise specified. Analytical thin layer chromatography (TLC) was performed with Macherey-Nagel Silica gel 60 UV_{254} aluminum plates and visualization was accomplished by UV light (254 nm) or staining with phosphomolybdic acid (PMA) followed by heating. Flash column chromatography was performed using Macherey-Nagel Silica gel 60 (230–400 mesh). Deuterated solvents were purchased from Cambridge Isotope Laboratories Inc.

Compound 1: Synthesis according to the modification of a reported procedure [64]. A mixture of 9-bromoro-1-nonanol (482 mg, 2.16 mmol) and sodium hydride (100 mg, 4.17 mmol) in dimethylformamide (5 mL) was stirred at 0 °C for 15 min. Propargyl

bromide (0.2 mL, 2.59 mmol) was added dropwise to the mixture solution and stirred at room temperature for 16 h. The resulting mixture was washed with brine (25 mL x 1), water (25 mL x 2) and brine (25 mL x 1). The combined organic layers were dried over sodium sulphate. The solvent was evaporated under vacuum and subjected to column chromatography on silica gel (hexane/ethyl acetate; v/v = 10/1, R_f = 0.5) to afford compound **1** as pale-yellow liquid (284 mg, 1.09 mmol) in 50% yield. ^{1}H NMR (600 MHz, $CDCl_3$) δ 4.08 (s, 2H), 3.46 (t, *J* = 6.6 Hz, 2H), 3.36 (t, *J* = 7.0 Hz, 2H), 2.39 (s, 1H), 1.80 (q, *J* = 7.3 Hz, 2H), 1.54 (t, *J* = 6.4 Hz, 2H), 1.37 (t, *J* = 7.4 Hz, 2H), 1.31 – 1.25 (m, 8H). HRMS (ESI+) calculated for $C_{12}H_{22}BrO$ $[M + H]^+$ 261.0849, found: 261.0848.

Compound 2: Synthesis according to the modification of a reported procedure [62]. ^{1}H NMR (600 MHz, CD_3SOCD_3) δ 8.19 (t, *J* = 8.0 Hz, 1H), 8.01 – 7.97 (m, 2H), 7.89 (d, *J* = 7.7 Hz, 2H), 7.70 (d, *J* = 7.2 Hz, 2H), 7.43 (t, *J* = 7.3 Hz, 2H), 7.32 (t, *J* = 7.6 Hz, 2H).

Compound 3: A mixture of compound **1** (87 mg, 0.33 mmol) and compound **2** (103 mg, 0.22 mmol) in the presence of a catalytic amount of copper(I) iodide (4 mg, 0.02 mmol) in triethylamine (1 mL) and dichloromethane (20 mL) was stirred at room temperature for 3 h. The resulting mixture was dried under vacuum and subjected to column chromatography on silica gel (hexane/dichloromethane; v/v = 1/2, R_f = 0.5) to afford compound **3** as yellow solid (109 mg, 0.16 mmol) in 71% yield. ^{1}H NMR (400 MHz, $CDCl_3$) δ 7.98 (d, *J* = 7.3 Hz, 2H), 7.83 (t, *J* = 7.9 Hz, 1H), 7.51 (d, *J* = 7.7 Hz, 2H), 7.43 (d, *J* = 7.9 Hz, 2H), 7.35 (t, *J* = 6.7 Hz, 2H), 7.22 (t, *J* = 7.6 Hz, 2H), 4.47 (s, 2H), 3.73 (t, *J* = 6.7 Hz, 2H), 3.38 (t, *J* = 6.9 Hz, 2H), 1.83 (p, *J* = 7.0 Hz, 2H), 1.76 – 1.64 (m, 2H), 1.42 (dt, *J* = 14.4, 7.6 Hz, 4H), 1.32 (q, *J* = 5.6 Hz, 6H). ^{13}C NMR (101

MHz, $CDCl_3$) δ 166.85, 165.10, 149.11, 142.35, 136.77, 132.06, 126.85, 125.27, 116.85, 96.68, 86.21, 77.36, 69.56, 60.35, 34.25, 33.00, 29.88, 29.59, 28.89, 28.34, 26.46. HRMS (ESI+) calculated for $C_{29}H_{32}AuBrNO$ $[M + H]^+$ 686.1328, found: 686.1319.

GA: A mixture of compound **3** (92 mg, 0.13 mmol) and 20% trimethylamine in ethanol (1 mL) in dichloromethane (2 mL) was heated at 50 °C for 24 h in a Schlenk Tube. The resulting mixture was cooled down to room temperature and precipitated with dichloromethane and diethyl ether. The precipitate was filtered off and was washed with hexane to afford **GA** as pale-yellow solid (69 mg, 0.09 mmol) in 69% yield. ^1H NMR (600 MHz, MeOD) δ 8.02 – 7.97 (m, 1H), 7.86 (d, *J* = 7.7 Hz, 2H), 7.70 (t, *J* = 7.9 Hz, 4H), 7.31 (t, *J* = 6.6 Hz, 2H), 7.27 – 7.21 (m, 2H), 4.40 (s, 2H), 3.73 (t, *J* = 6.3 Hz, 2H), 3.26 (s, 2H), 3.08 (s, 9H), 1.76 (q, *J* = 8.0 Hz, 2H), 1.69 (q, *J* = 7.1 Hz, 2H), 1.48 (d, *J* = 7.1 Hz, 2H), 1.38 (d, *J* = 25.2 Hz, 8H). ^{13}C NMR (151 MHz, MeOD) δ 167.70, 166.23, 150.82, 144.43, 137.36, 132.60, 128.01, 126.67, 118.53, 70.40, 60.99, 53.43, 30.61, 30.40, 30.28, 30.06, 27.29, 23.88. HRMS (ESI+) calculated for $C_{32}H_{40}AuN_2O$ $[M – Br]^+$ 665.2801, found: 665.2846.

Preparation of Aqueous Sample: GA (13.4 mM, 1.0 wt.%) was dissolved in fresh MilliQ water (MQ water). The solution was heated at 50.0 °C for 5 min, then slowly cooled to 20.0 °C at a rate of 1.0 °C/min to form assembled structure.

UV-vis Spectroscopy: UV-vis measurements were performed on Agilent Cary 60 UV-visible Spectrophotometer with a 1 cm path length quartz cuvette. A Luma 40/8453 temperature-controlled cuvette holder with four optical ports was mounted in the sample compartment of Agilent Cary 60 UV-visible spectrophotometer. Time-

dependent UV-vis adsorption measurements were performed using a small stirring bar (3*5 mm) at a constant stirring speed of 1200 rpm. Slits were installed on the cuvette holder to prevent the stirring bar from interfering with the optical path to the spectrometer. Measurement of all samples were carried out at 20.0 °C unless otherwise specified.

Fluorescence Spectroscopy: Fluorescence measurements were performed on an Agilent G9800A Cary Eclipse fluorescence spectrophotometer with a 1 cm path length quartz cuvette. A Luma 40/8453 temperature-controlled cuvette holder with four optical ports was mounted in the sample compartment of Agilent G9800A Cary Eclipse fluorescence spectrophotometer. Measurement of all samples were carried out at 20.0 °C unless otherwise specified.

Static Light Scattering (SLS): Static Light Scattering intensities of each sample were determined on a Wyatt Technology DynaPro NanoStar. The scattering intensities were recorded as a parameter for assembly size, given that the objects in solution are anisotropic and the models used by Wyatt software are fitting for spherical objects. The critical aggregation concentration (CAC) of **GA** is determined by the scattering intensities of the solutions of **GA** (concentration: 0.01 to 1.0 mM) at 20.0 °C. The scattering rate was normalized by the concentration of the solution to yield the molar scattering intensity (M Counts s^{-1} M^{-1}). Ten replications were performed, and the data was averaged to show the molar scattering intensity and corresponding standard deviation.

Incubation of GA with Sodium Tosylate for Counter Anion Controlled Supramolecular Transformation: A thermal annealed aqueous solution of **GA** (13.4

mM) was added with an aqueous solution of sodium tosylate (1.0, 2.0, and 4.0 equiv.). The obtained solution was incubated at 50.0 °C for 5 min, and slowly cooled down to 20.0 °C at a rate of 1.0 °C/min.

Transmission Electron Microscopy (TEM): TEM sample was prepared by depositing sample solutions (0.2 wt.%, 10.0 μL) onto a carbon grid (Micro to Nano, EMR Carbon support film on copper, 400 square mesh) for 30 s. The sample solution was removed by blotting and UranyLess EM stain solution (Electron Microscopy Science, 5.0 μL) was directly deposited onto the grid for 15 s, and the stain was removed by blotting. Grids were observed in a ThermoFisher Talos L120C Transmission Electron Microscope at an accelerating voltage of 120 kV. TEM images were captured on a Ceta 16M CCD camera.

Atomic Force Microscopy (AFM): The atomic force microscopy was performed on a JPK NanoWizard V BioScience AFM (Bruker) equipped on Nikon ECLIPSE Ti-2 microscope with a cantilever (RFESPG-75, Bruker). The measurement of the assembled morphology was conducted in air with Peakforce Tapping mode. The sample solution (0.2 wt.%, 5.0 μL) was dropped onto a freshly cleaved mica plate surface and spin-coated to remove excess solvent.

Supporting Information

Supporting Information File 1:

File Name: SI-BLOC-GA

File Format: PDF

Title: Experimental details, supporting figures, and copies of spectra.

Acknowledgements

We acknowledge the technical support from UCEA and ULS of PolyU.

Funding

This work was supported financially by the Hong Kong Research Grants Council General Research Fund (GRF 15305822) and the Hong Kong Polytechnic University (BC7W, CDMU, WZCT, WZCA) for F. K.-C. Leung.

References

1. Simmons, N. S.; Blout, E. R. *Biophys. J.* **1960**, *1* (1), 55-62.
2. Lino, T. *J. Supramol. Struct.* **1974**, *2* (2-4), 372-384.
3. Chapman, D. *Q. Rev. Biophys.* **1975**, *8* (2), 185-235.
4. Aida, T.; Meijer, E.; Stupp, S. *Science* **2012**, *335* (6070), 813-817.
5. Krieg, E.; Bastings, M. M.; Besenius, P.; Rybtchinski, B. *Chem. Rev.* **2016**, *116* (4), 2414-2477.
6. Feringa, B. L. *Angew. Chem., Int. Ed.* **2017**, *56* (37), 11060-11078.
7. Chen, S.; Costil, R.; Leung, F. K.-C.; Feringa, B. L. *Angew. Chem., Int. Ed.* **2021**, *60* (21), 11604-11627.
8. Israelachvili, J. N.; Mitchell, D. J.; Ninham, B. W. *J. Chem. Soc., Faraday Trans. 2* **1976**, *72* (9), 1525.
9. Degiorgio, V. *Europhys. News* **1985**, *16* (6), 9-12.
10. Feringa, B. L. *J. Org. Chem.* **2007**, *72* (18), 6635-6652.

11. Shigemitsu, H.; Fujisaku, T.; Tanaka, W.; Kubota, R.; Minami, S.; Urayama, K.; Hamachi, I. *Nat. Nanotechnol.* **2018**, *13* (2), 165-172.
12. Dattler, D.; Fuks, G.; Heiser, J.; Moulin, E.; Perrot, A.; Yao, X.; Giuseppone, N. *Chem. Rev.* **2019**, *120* (1), 310-433.
13. Baroncini, M.; Silvi, S.; Credi, A. *Chem. Rev.* **2019**, *120* (1), 200-268.
14. Volarić, J.; Szymanski, W.; Simeth, N. A.; Feringa, B. L. *Chem. Soc. Rev.* **2021**, *50* (22), 12377-12449.
15. Leung, F. K.-C. Aqueous Supramolecular Assemblies of Photocontrolled Molecular Amphiphiles. In *Supramolecular Assemblies Based on Electrostatic Interactions*; Aboudzadeh, M. A.; Frontera, A., Eds.; Springer International Publishing: Cham, 2022; pp 267-308.
16. Cheung, L.-H.; Liu, B. B.; Leung, F. K.-C. *Polym. J.* **2023**, *55* (11), 1189-1198.
17. Chau, A. K.-H.; Leung, F. K.-C. *Adv. Colloid Interface Sci.* **2023**, *315*, 102892.
18. Cheung, L.-H.; To, J. C.; Wong, W.-K.; Stuart, M. C. A.; Kajitani, T.; Keng, V. W.; Leung, F. K.-C. *ACS Appl. Mater. Interfaces* **2024**, *16* (3), 4056-4070.
19. Hung, K.-L.; Cheung, L.-H.; Ren, Y.; Chau, M.-H.; Lam, Y.-Y.; Kajitani, T.; Leung, F. K.-C. *Beilstein J. Org. Chem.* **2024**, *20*, 1590-1603.
20. Yau, J. C.-K.; Hung, K.-L.; Ren, Y.; Kajitani, T.; Stuart, M. C. A.; Leung, F. K.-C. *J. Colloid Interface Sci.* **2024**, *662*, 391-403.
21. Meng, J.; Cheung, L.-H.; Ren, Y.; Stuart, M. C. A.; Wang, Q.; Chen, S.; Chen, J.; Leung, F. K.-C. *Macromol. Rapid Commun.* **2024**, *45* (17), 2400261.
22. Chau, M.-H.; Wong, W.-K.; Kajitani, T.; Leung, F. K.-C. *Adv. Sci.* **2024**, *11* (45), 2407130.
23. Chau, M.-H.; Wong, W.-K.; Meng, S.; Kajitani, T.; Leung, F. K.-C. *Dyes Pigm.* **2024**, *230*, 112334.

24. Wycisk, V.; Wagner, M.-C.; Urner, L. H. *ChemPlusChem* **2024**, *89* (1), e202300594.

25. Hung, K.-L.; Wong, W.-K.; Chau, M.-H.; Yau, J. C.-K.; Kajitani, T.; Chen, S.; Leung, F. K.-C. *ACS Appl. Nano Mater.* **2025**, *8* (17), 8876-8885.

26. Cheung, L.-H.; Leung, F. K.-C. *Chem. Eur. J.* **2025**, *31* (33), e202500791.

27. Yau, J. C.-K.; Leung, F. K.-C. *J. Organomet. Chem.* **2025**, *1031*, 123596.

28. Liu, B. B.; Zhang, H.; Wong, W.-K.; Chau, M.-H.; Cheung, L.-H.; Kajitani, T.; Leung, F. K.-C. *Small* **2025**, *21* (32), 2503359.

29. Meng, S.; Chau, M.-H.; Kajitani, T.; Leung, F. K.-C. *Adv. Robot. Res.* **2025**, *n/a* (n/a), e202500070.

30. Yau, J. C.-K.; Chen, C. Y.; Zhang, H.; Chau, M.-H.; Kajitani, T.; Leung, F. K.-C. *Mater. Chem. Front.* **2025**, *9* (23), 3414-3424.

31. Ren, Y.; Cheung, L.-H.; Kajitani, T.; Leung, F. K.-C. *J. Colloid Interface Sci.* **2026**, *702* (Part_1), 138850.

32. Lee, T. H.-W.; Hung, K.-L.; Kajitani, T.; Leung, F. K.-C. *ChemPhotoChem* **2026**, *10* (2), e202500333.

33. Zhang, H.; Cai, K. S.-Y.; Liu, B. B.; Huang, J.; Leung, F. K.-C. *Langmuir* **2026**.

34. Leung, F.; Hung, K.-L.; Wong, W. K. R.; Cheung, L.-H.; Chau, M.-H.; Kajitani, T. *Res. Sq.* **2025**.

35. Yin, B.; Wong, W.-K.; Ng, Y.-M.; Yang, M.; Leung, F. K.-C.; Wong, D. S.-H. *Pharmaceutics* **2023**, *15* (5), 1427.

36. Wong, W.-K.; Ren, Y.; Leung, F. K.-C. Chapter 16 - Photothermal-chemotherapy: the emerging supramolecular photothermal molecules and the recent advances. In *Nanophototherapy*; Manivasagan, P.; Venkatesan, J.; Jang, E.-S., Eds.; Elsevier: 2025; pp 463-499.

37. Owen, T.; Butler, A. *Coord. Chem. Rev.* **2011**, *255* (7-8), 678-687.

38. Muñoz, M. J. M.; Fernández, G. *Chem. Sci.* **2012**, *3* (5), 1395-1398.

39. Fu, H. L.-K.; Yam, V. W.-W. *Chem. Lett.* **2018**, *47* (5), 605-610.

40. Yam, V. W. W.; Law, A. S. Y. *J. Chin. Chem. Soc.* **2020**, *67* (12), 2246-2252.

41. Poon, J. K.-L.; Chen, Z.; Leung, S. Y.-L.; Leung, M.-Y.; Yam, V. W.-W. *Proc. Natl. Acad. Sci.* **2021**, *118* (6), e2022829118.

42. Zi, W.; Toste, F. D. *Chem. Soc. Rev.* **2016**, *45* (16), 4567-4589.

43. Cui, J. F.; Ko, H. M.; Shing, K. P.; Deng, J. R.; Lai, N. C. H.; Wong, M. K. *Angew. Chem., Int. Ed.* **2017**, *129* (11), 3120-3125.

44. Rocchigiani, L.; Bochmann, M. *Chem. Rev.* **2020**, *121* (14), 8364-8451.

45. Yam, V. W.-W.; Chan, A. K.-W.; Hong, E. Y.-H. *Nat. Rev. Chem.* **2020**, *4* (10), 528-541.

46. Tang, M.-C.; Chan, M.-Y.; Yam, V. W.-W. *Chem. Rev.* **2021**, *121* (13), 7249-7279.

47. Kung, K. K.-Y.; Ko, H.-M.; Cui, J.-F.; Chong, H.-C.; Leung, Y.-C.; Wong, M.-K. *Chem. Commun.* **2014**, *50* (80), 11899-11902.

48. Sit, H.-Y.; Yang, B.; Ka-Yan Kung, K.; Siu-Lun Tam, J.; Wong, M.-K. *ChemPlusChem* **2019**, *84* (11), 1739-1743.

49. Ko, H.-M.; Deng, J.-R.; Cui, J.-F.; Kung, K. K.-Y.; Leung, Y.-C.; Wong, M.-K. *Bioorg. Med. Chem.* **2020**, *28* (7), 115375.

50. Wang, F.; Lan, M.; To, W.-P.; Li, K.; Lok, C.-N.; Wang, P.; Che, C.-M. *Chem. Commun.* **2016**, *52* (90), 13273-13276.

51. Wan, Q.; Xia, J.; Lu, W.; Yang, J.; Che, C.-M. *J. Am. Chem. Soc.* **2019**, *141* (29), 11572-11582.

52. Leung, M.-Y.; Leung, S. Y.-L.; Yim, K.-C.; Chan, A. K.-W.; Ng, M.; Yam, V. W.-W. *J. Am. Chem. Soc.* **2019**, *141* (49), 19466-19478.

53. Yam, V. W. W.; Choi, S. W.; Lai, T. F.; Lee, W. K. *J. Chem. Soc., Dalton Trans.* **1993**, (6), 1001.

54. Yam, V. W.-W.; Wong, K. M.-C.; Hung, L.-L.; Zhu, N. *Angew. Chem., Int. Ed.* **2005**, *44* (20), 3107-3110.

55. Wong, K. M.-C.; Zhu, X.; Hung, L.-L.; Zhu, N.; Yam, V. W.-W.; Kwok, H.-S. *Chem. Commun.* **2005**, (23), 2906-2908.

56. Wong, K. M.-C.; Hung, L.-L.; Lam, W. H.; Zhu, N.; Yam, V. W.-W. *J. Am. Chem. Soc.* **2007**, *129* (14), 4350-4365.

57. Au, V. K.-M.; Wong, K. M.-C.; Zhu, N.; Yam, V. W.-W. *J. Am. Chem. Soc.* **2009**, *131* (25), 9076-9085.

58. Au, V. K.-M.; Wong, K. M.-C.; Tsang, D. P.-K.; Chan, M.-Y.; Zhu, N.; Yam, V. W.-W. *J. Am. Chem. Soc.* **2010**, *132* (40), 14273-14278.

59. Jiang, J.-J.; Chau, A. K.-H.; Wong, M.-K.; Leung, F. K.-C. *Eur. J. Inorg. Chem.* **2022**, *2022* (24), e202200281.

60. Chau, M.-H.; Chan, A. K.-H.; Ren, Y.; Jiang, J.-J.; Wong, M.-K.; Leung, F. K.-C. *J. Organomet. Chem.* **2023**, *999*, 122827.

61. Chan, A. K.-H.; Chau, M.-H.; Ren, Y.; Jiang, J.-J.; Wong, M.-K.; Leung, F. K.-C. *ChemPlusChem* **2024**, *89* (2), e202300316.

62. Wong, K.-H.; Cheung, K.-K.; Chan, M. C.-W.; Che, C.-M. *Organometallics* **1998**, *17* (16), 3505-3511.

63. Liu, S.; Gonzalez, Y. I.; Danino, D.; Kaler, E. W. *Macromolecules* **2005**, *38* (6), 2482-2491.

64. Chen, J.; Wang, J.; Bai, Y.; Li, K.; Garcia, E. S.; Ferguson, A. L.; Zimmerman, S. C. *J. Am. Chem. Soc.* **2018**, *140* (42), 13695-13702.